CENTERIS - International Conference on ENTERprise Information Systems / ProjMAN - International Conference on Project MANagement / HCist - International Conference on Health and Social Care Information Systems and Technologies, CENTERIS/ProjMAN/HCist 2018

# Accuracy of Sentinel-1 Interferometry Monitoring System based on Topography-free Phase Images

Milan Lazecký[a,*], Ivana Hlaváčová[b], Jan Martinovič[a], Antonio Miguel Ruiz-Armenteros[c,d,e]

*a IT4Innovations, VSB-TU Ostrava, 17. listopadu 15, 708 33 Ostrava-Poruba, Czech Republic*
*b GISAT Ltd., Milady Horakove 57, 170 00 Praha 7, Czech Republic*
*c Dpto. Ingeniería Cartográfica, Geodésica y Fotogrametría, Univ. Jaén, EPSJ, Campus Las Lagunillas s/n, Edif. A3, 23071 Jaén, Spain*
*d Centro de Estudios Avanzados en Ciencias de la Tierra CEACTierra, Universidad de Jaén, Spain*
*e Grupo de investigación Microgeodesia Jaén, Universidad de Jaén, Spain*

## Abstract

Our automatized interferometric monitoring system, IT4S1, contains a database of Sentinel-1 satellite image bursts that have been preprocessed to the state of a consistent well-coregistered dataset. The coregistration solution introduces a new type of data, an SLC-C (corrected single look complex data). These are SLC images ready for interferometric analyses with maximally reduced phase signature of topography and flat-Earth phase. The further processing time for multitemporal interferometry techniques is significantly reduced for achieving velocity maps based on e.g. Persistent Scatterers or Small Baseline techniques.

In this paper, authors focus on quality of estimated topographic phase, finding out that computation of perpendicular baseline between satellite positions based on precise orbit ephemerides can differ and thus the approach may suffer from a residual topographic signature or a flat-Earth phase. The paper presents conclusions taken by an investigation of one such pre-prepared dataset over a mountainous area in southern Spain. Though some orbital inparallelity occurs during Sentinel-1 acquisitions (causing inaccuracies of perpendicular baselines within first meters), the flat-Earth is removed properly using this approach.

The paper further demonstrates results using SLC-C approach using available and custom processing techniques and notifies about the possibility that in terms of overall accuracy and precision of multitemporal interferometry this approach contains inaccuracies that can be either estimated as part of error phase screens or even neglected.

* Corresponding author. Tel.: +420 776 562 313.
  E-mail address: milan.lazecky@vsb.cz

## 1. Introduction

In order to process Sentinel-1 Synthetic Aperture Radar (SAR) standard interferometric wide swath (IWS) images, the data should be coregistered to a perfect fit in accuracy of a 0.001 pixel[1]. This is performed using a typical image coregistration processing followed by correction of phase ramps caused within the specific mode of image acquisition called Terrain Observation by Progressive Scans (TOPS)[2] – this operation is known as Enhanced Spectral Diversity (ESD)[1]. This is usually the step where the most of the SAR interferometry (InSAR) systems stop in preprocessing their data before generating interferograms.

An interferogram is basically created by a complex conjugate of two well-coregistered SAR images (i.e. their phase difference is generated). An interferogram image contains information from various sources influencing the radar phase, the two major sources of interest being a physical displacement that happened between the image acquisitions and a phase signal induced by height difference due to stereoscopic effect of a differing satellite position during acquiring images.

If the goal is to identify displacements of observed targets, it is necessary to remove all other components from the interferogram. For example, a phase change induced by topography can be removed using a digital elevation model (DEM) recomputed into the specific SAR line of sight (LOS) taking into account the perpendicular baseline ($B_{perp}$) between both satellite positions. This is normally performed during generation of interferograms since $B_{perp}$ is unique within each acquisition pair. The generation of topographic phase screen is computationally relatively demanding and not very effective in case of needs of processing large number of interferograms for multitemporal SAR interferometry (MT-InSAR). Some approaches prepared effective solutions, e.g. SARproZ[3] that computes topography phase during the processing chain for only selected MT-InSAR points – this improves the situation for Permanent Scatterers (PS)[4] MT-InSAR processing but not for e.g. the Small Baselines (SB)[5] technique where spatially filtered topography-free interferogram is an advantage.

The IT4S1 system solution[6] shows another alternative, that is, to remove topography signal already from the SLC image and thus generating the final product - a corrected/calibrated SLC image (SLC-C). Basically the principle is to generate a synthetic phase from a DEM towards a master image based on its look angle defining its LOS. Precise orbit information is a pre-requisite of a success of this step and this is secured by current ESA precise orbit ephemerides (POD) products[7]. This solution should find advantages in both PS and SB processing approaches.

Within IT4S1, during the coregistration process so-called fine offsets in both range and azimuth directions are created by NASA/JPL ISCE software package[8] that describes the misalignment of both images pixelwise. The computed topographic effect is included in these offsets. By removing these offsets from the phase difference, an interferogram is formed. However, by removing the offsets only from the slave image, this image will achieve the state of precisely coregistered image with topography-based signal removed (or at least maximally reduced). Since the orbital tube of Sentinel-1 is relatively narrow (the statistical root mean square of the orbital tube[9] is 50 m causing a height ambiguity of up to 300 m per a phase cycle which can be considered relatively low sensitivity to height), the removal of topography effect based on the combination of only two images should be relatively safe, though some residual topography should be accounted for.

## 2. Baseline inaccuracy influence

The length of the perpendicular baseline is used more times during the interferogram creation process (e.g. the DEM-refined coregistration). Inaccuracy of its estimation influences the interferogram significantly in two steps - in the subtraction of the flat-Earth (Eq. 1) and topographic (Eq. 2) phase components.

$$\Phi_{fE} = \frac{4\pi}{\lambda} B_{par} \tag{1}$$

$$\Phi_{topo} = \frac{4\pi}{\lambda} B_{perp} \frac{h}{R\sin\theta} \tag{2}$$

where $\lambda$ is the radar wavelength, $B_{par}$ is the parallel baseline, $B_{perp}$ is the perpendicular baseline, $h$ is the height of the scatterer over the reference surface (due to the fact that InSAR gives relative results, the height can be taken w.r.t. any altitude, constant within an image), $R$ is the slant range and $\theta$ is the incidence angle of the radar.

As the length of the parallel baseline changes heavily along the range coordinate, it is not usually disclosed, but the frequency of flat-Earth fringes in the range direction is related to the perpendicular baseline (Eq. 3)

$$f = \frac{d\Phi}{d\theta} = -\frac{4\pi}{\lambda} B_{perp} \tag{3}$$

where $B_{perp}$ changes in the range direction only slightly and its changes are usually neglected.

When subtracting an inaccurate flat-Earth phase, some of the flat-Earth fringes stay in the interferogram: we will call these the residual fringes and label their frequency $df$. The value $df = 1$ means that the residual phase $d\Phi$ changes by 1 rad when the look angle $\theta$ changes by 1 rad.

Within one swath, the radar incidence angle of Sentinel-1 changes by 5.5 degrees[10], and in this range, the influence on the flat-Earth phase can be assumed linear (the nonlinearities can be neglected).

The residual fringe frequency $df$ (which should be 0 ideally) is therefore

$$df = -\frac{4\pi}{\lambda} dB_{perp} \tag{4}$$

where $dB_{perp}$ is the perpendicular (with respect to the radar beam direction) component of the error baseline vector. The residual fringe frequency does not depend on the baseline itself, but only on the residual perpendicular baseline.

Applied to our problem, if two slave images are coregistered to one master and their perpendicular baselines are calculated also w.r.t. this master, residual flat-Earth (and topographic) fringes may be present in the interferogram generated from these two slaves (without the master image). Equation 5 describes this situation as the sum of the combination of $dB_{perp}$ residuals between A,B,C images (where A is a master image) is generally not exactly 0.

$$dB_{perp, A-B} + dB_{perp,B-C} - dB_{perp, A-C} = \sim 0 \tag{5}$$

Our problem is now to estimate the baseline error $dB_{perp,B-C}$ (as the other two baseline errors are computed directly from orbits and are therefore subject to only orbit errors), computed from Eq. 4.

We generated about 310 000 image triples of Sentinel-1 data from over 100 images of one burst and calculated the baselines of the three pairs within each triple, to estimate the residual baseline originating from the computation of an interferogram between two DEM-removed slave images. Standard deviation of the computed $B_{perp}$ for this dataset is 5.1 m. For such a residual baseline, the flat-Earth ramp over the whole swath (in range) would be 17.5 phase cycles. However, for many of the image triples, the residual baseline is in the order of cm or even mm (comparable to the orbit error inaccuracy), where no visible phase ramps are expected. We attribute the significantly non-zero sums to the inparallelness of the orbits, explaining why this happens only for some of the triples. During the coregistration, the images are rotated in order to be parallel, and then, the baseline sums are zero in the triplet. That means that for the interferometric evaluation (including multitemporal InSAR analyses), coregistration-corrected baselines are to be used.

Our approach therefore includes usage of orbit data of a master image (where all images are coregistered to and which was used for generation of DEM-based phase screen for topography phase removal) instead of original orbit

data of each image in the process of the update of SLC-C dataset. An example of a generated interferometric combination using this approach is shown in Fig. 1. Here the classic approach has been used to generate an interferogram using SARproZ[11] over a hilly area of southern Spain (with height difference of over 3 000 m) from the well-coregistered dataset (with and without usage of DEM for topography phase removal), while the approach of generating interferogram from SLC-C data shows a very similar topography-free interferogram.

Note that the $B_{perp}$ = 160 m (height ambiguity reaches 94 m per a phase cycle) for this configuration of images from 2017-03-05 and 2017-03-11. No significant residual flat-Earth phase ramp is visible in this interferogram – triplets using these data keep the average (median) $dB_{perp}$ = 0.2 m with extremes such as $dB_{perp}$ = 3.176 m in a triplet combination of these images with 2017-02-11 image.

Theoretically such error can cause 10 fringes in the flat-Earth ramp (based on Eq. 3 and 4 related to whole maximum of 5.5° look angle variation within the burst), however in practice no significant residual flat-Earth phase has been detected in this interferogram. Height ambiguity for such error is 1 fringe within the investigated ~3 000 m height difference - such error can be neglected since the residual topography can be modeled and corrected in further multitemporal InSAR analyses and is also comparable or lower than the elevation-dependent pressure changes affecting the radar signal.
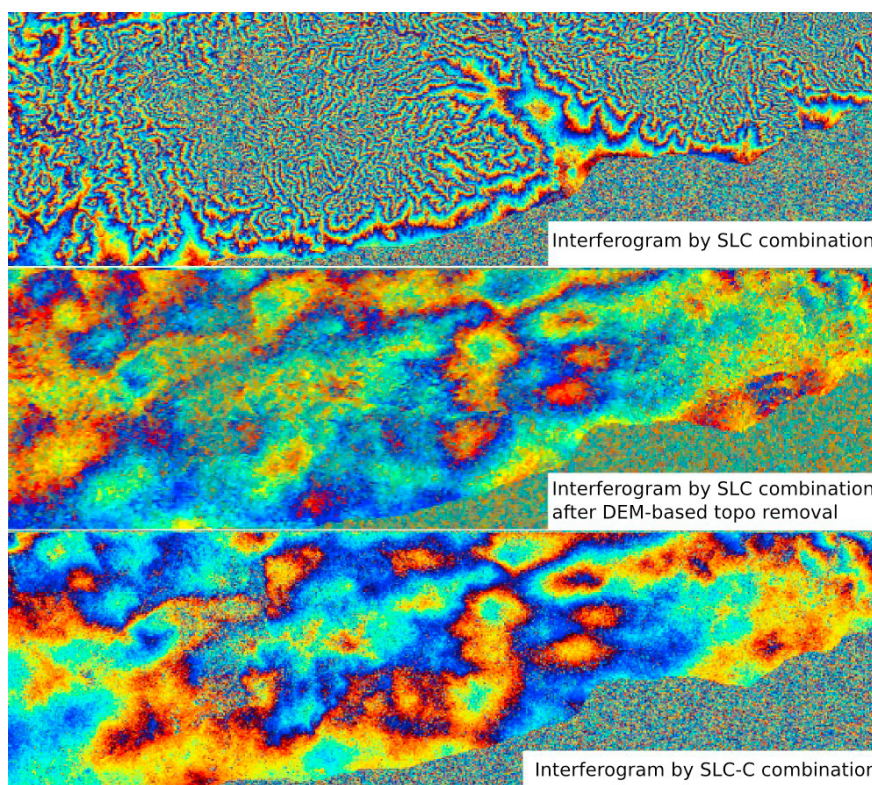


Fig. 1. Burst interferogram generation by complex conjugate of coregistered SLC images (upper) and followed by a convenient topography removal using DEM-based topography screen (middle). Proposed solution using topography-free SLC-C data shown below. The dataset is from 2017-03-05 and 2017-03-11 with $B_{perp}$=160 m

## 4. Accuracy and precision of the InSAR method

Geodesists often request information about the accuracy of InSAR measurements. Unfortunately, ground-truth data are often unavailable, and if available, validation is often possible only for few points of the processed area.

Moreover, the recognition of the reflecting objects is not always possible, especially for pixels with lower coherence which are of interest when monitoring e.g. a landslide.

As a measure of reliability, coherence is normally used in InSAR. Coherence is by definition the property of a pixel/feature, not of the data[17]. Therefore, the coherence evaluated from the data is a statistical estimation and therefore depends on the dataset properties: number of images, spatial and temporal baselines. Also, it heavily depends on the appropriateness of the model that has been used to estimate the physical displacements. For example, if only linear velocities are estimated or if other parameters are included such as temporal variation of the motion (e.g. if dam movements correspond to water levels, or gas storages cause subsidence and uplift related to ingestion and discharge periods, etc.) – in the latter case, an appropriate accuracy of the external data should be secured. If the model is inappropriate for the given point, the coherence is underestimated.

Adding other parameters (such as thermal dilation in case of bridge monitoring[18] or water level influence in case of monitoring dam displacements[19]) to the model makes it usually more appropriate if enough data are processed. The number of available Sentinel-1 images is now usually high enough.

If the estimation of parameters (velocity, height correction, possibly others) is performed with the use of a Fast Fourier Transformation (FFT) method, the coherence is maximized for a point. Some software use a least-squares (LS) method for parameter estimation, where the standard deviation of phase residues is minimized instead. These are two different criteria, giving slightly different results.

The formula to relate the coherence to the phase standard deviation is[17]

$$\sigma = \sqrt{-2\,ln\gamma} \qquad (6)$$

but does not apply accurately, and also, the residues are generally different when estimated using the two criteria. According to our experiments, LS methods are more sensitive to outliers caused e.g. by snow cover or strong atmospheric phase screen (APS), while coherence better estimates the noise of the reflecting pixel. On the other hand, geodetists require the standard deviation, and moreover, standard deviation is necessary to decide reliably if a reflector moves.

According to our experiments, the rate between the standard deviation evaluated by (6) from the coherence, and the standard deviation evaluated as the root mean square (RMS) of the residues (evaluated using the same criteria) is between 0.8-1.2, with the peak approximately at 1.

In the following, we call the evaluated velocity standard deviation the precision, no matter the optimization criteria is. Let us stress here that it reflects how the data correspond to the a-priori model.

On the other hand, accuracy represents how the estimated parameters meet the reality. Mostly, this is not possible to estimate due to the cost of the geodetic measurements, and if available, it is only possible for few (well-coherent) points.

Our experiment tries to evaluate the accuracy of the method based on the assumption of the stability of a selected area. The velocity precision depends on the quality of a point (coherence) and dataset properties[17], with

$$\sigma_v \approx \frac{\lambda}{4\pi}\frac{\sigma}{\sqrt{n}\cdot\delta_{\Delta T}} \qquad (7)$$

where *n+1* is the number of images and $\delta_{\Delta T}$ is the variance of temporal baselines. The accuracy is expected to depend on the same parameters, and, ideally, it is expected to have a similar value as the precision.

We process an area assumed to be stable, divide the processed points into groups according to the evaluated coherence, and calculate the standard deviation of the estimated velocity in each group, assuming the "correct" velocity of each point to be 0. Within the calculation, outliers are excluded (not iteratively).

This way, we get an estimate of the accuracy, but not for each point, but for a coherence interval (or the evaluated precision). It is an area estimate. We suppose that a similar accuracy should apply to points processed in the same dataset, but different (non-stable) areas of interest.

Figure 6 shows the results of our experiment: the relation between precision and accuracy for three software packages: SARPROZ(c) (127 images), STAMPS (113 images) and SALSIT (113 images), together with the number of points over the coherence threshold (estimated to be reliable). The area processed is the same, a part of the city of Prague, Czech republic (approximately half of a burst), with the number of points between 25 000-100 000.
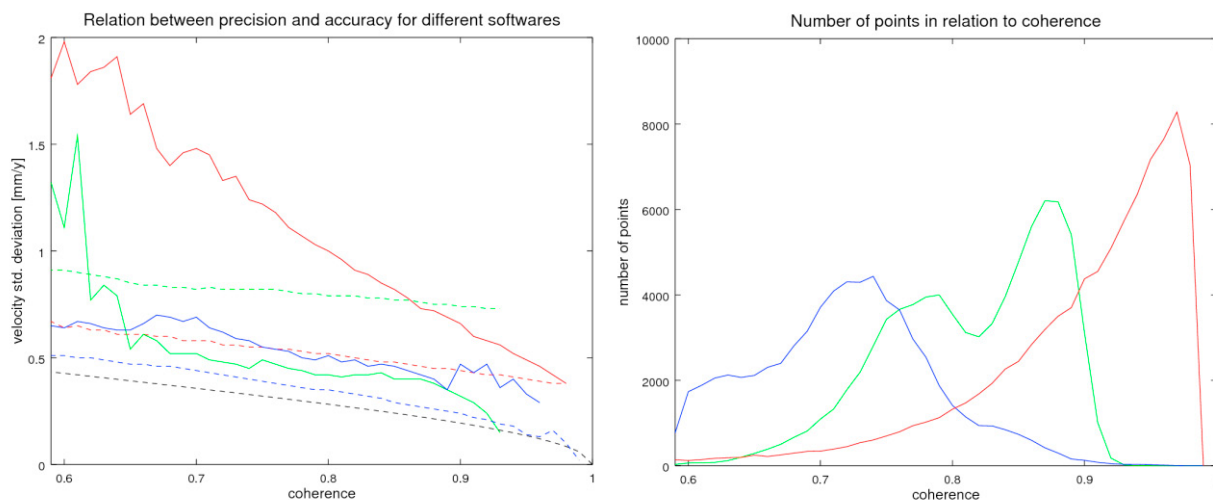


Fig. 2. Relation between the velocity precision (dashed lines) and accuracy (solid lines) for different coherence values (left) and a number of points in relation to their coherence (right), estimated in three different software packages: SARPROZ(c) (green, 127 images), STAMPS (red, 113 images) and SALSIT (blue, 113 images). The black line (left) is the theoretical precision, based on coherence. The processing area is the Prague city. During processing, atmospheric phase screen (APS) was not removed.

From Fig. 2, one can see that SARPROZ(c), using the FFT methods, has the best accuracy for most of the points, but if coherence drops to about 0.62, there are many points with phase unwrapping errors, enlarging the velocity standard deviation. On the other hand, the velocity precision, estimated as the width of the periodogram[21], significantly overestimates the accuracy.

High accuracy values for the STAMPS software can be probably attributed to phase filtering, stronger with lower coherence, and also to an inappropriate estimation of coherence (see below).

Regarding the distribution of points with regard to coherence, we can take SARPROZ (green line) as a reference, as this is the only software maximizing the coherence (the other two use LS method). Therefore, the coherence estimated by STAMPS seems to be unreliable, as not so many points should have such a good coherence (see Fig. 2 right - red line). The SALSIT number of points is easily understandable, as coherence is not maximized by LS.

For the decision if a point is to be taken as reliable, noise is not the key problem, as the velocity estimation is expected to be subject to a random error. The key problem are the ambiguities (phase unwrapping errors) which, if estimated incorrectly, can bias the estimated velocity significantly, far out of the velocity standard deviation value.

With a large data archive of Sentinel-1, one can afford to make large datasets where the probability of incorrect ambiguity estimation is much lower than for small datasets, and can afford to lower the coherence threshold to as minimal as possible. In the following, we will evaluate the coherence threshold value for different number of images.

Considering the phase noise to be normally distributed with the standard deviation of σ, and trying to avoid the phase noise to exceed the half of phase ambiguity with the probability of 99.7 %, we get the requirement shown in Equation 8:

$$\sigma \cdot \frac{\lambda}{4\pi} \leq \frac{\lambda}{12} \Rightarrow \sigma \leq \frac{\pi}{3}$$

$$(8)$$

, corresponding to the coherence of 0.58. According to the relation between coherence and phase standard deviation (6), and according to the fact that the coherence is a statistical estimation with the standard deviation of [17] (this formula applies only for PS, therefore for points with high coherence),

$$\sigma_\gamma = \frac{1}{\sqrt{2N}}(1 - e^{-\sigma^2}) = \frac{1}{\sqrt{2N}}(1 - \gamma^2)$$

.

*(9)*

Allowing the probability of 2.3 %, that the real coherence of the point is lower than the value of 0.58, the coherence threshold can be chosen on the basis of Table 1.

Table 1: Recommended values of coherence threshold for various number of images in a dataset

| number of images in dataset | 20 | 40 | 60 | 80 | 100 | 120 |
|---|---|---|---|---|---|---|
| coherence threshold | 0.727 | 0.694 | 0.677 | 0.666 | 0.658 | 0.652 |

However, setting the coherence threshold to 0.6 (allowing to interpret more points e.g. in an incoherent landslide area), the amount of points with incorrectly estimated ambiguities is quite low and these can be usually well recognized either in comparison to their surroundings, or based on their time series. For datasets with more than 100 images, this seems to apply also for the value of 0.5.

## 5. Conclusions

Advantages of the ISCE-based approach to generate topography-free SLC data (SLC-C) from Sentinel-1 images for the usage in InSAR analyses were presented in the paper. While the SLC-C generation can be relatively demanding for a computational power, such images can yield very fast interferometric combinations (usage of SLC-C dramatically decrease computational burden). This is a great advantage in using any (MT-)InSAR techniques. Subtle variation in topography has been indeed identified, however such residual phase can be further estimated and removed for selected points using common MT-InSAR techniques. We have investigated present orbital inaccuracies of S-1 that can yield a high number of residual flat-Earth fringes. These were not identified in generated interferograms thus we claim that the flat-Earth signal was successfully removed during SLC-C generation, together with the majority of the topographic signal. Our MT-InSAR[22,23] tests did not show significant differences between standard MT-InSAR approach and MT-InSAR processing starting from SLC-C images.

The whole IT4S1 system consists in the implementation of a SLC-C processor and MT-InSAR techniques, currently by StaMPS with parameters set for a generally acceptable performance and optimized to be used in an environment offering advanced parallel processing. A custom approach of PS InSAR implementation (SALSIT) has been prepared with the intention of keeping properties of InSAR as a geodetic method. In comparison to geodetical measurements, InSAR has several specific differences, e.g. relatively high noise, especially for low-reflectivity areas. This noise is compensated with the number of measurements in time (together with good spatial coverage, i.e. the density of points), in case an appropriate model is used for processing.

## Acknowledgements

purposes. Sentinel-1A/B data were freely provided by ESA through Copernicus Programme. Sentinel-1 precise orbit ephemerides were acquired from ESA Sentinel-1 Quality Control group.

# References

[1] Yague-Martinez, N., P. Prats-Iraola, F. Gonzalez, R. Brcic, R. Shau, D. Geudtner, M. Eineder, and R. Bamler. (2016) "Interferometric Processing of Sentinel-1 TOPS Data", *IEEE Trans. on Geos. and Rem. Sens*, **54**: 1-15, doi: 10.1109/TGRS.2015.2497902.

[2] De Zan, F. and Guarnieri, A. M. (2006) "TOPSAR: Terrain Observation by Progressive Scans. Geoscience and Remote Sensing", *IEEE Transactions on Rem. Sen.*, **44 (9)**: 2352–2360. doi:10.1109/TGRS.2006.873853

[3] Perissin, D., Wang, Z., Wang, T.. (2001) "The SARProZ InSAR tool for urban subsidence/manmade structure stability monitoring in China". In: Proceedings of 34th International Symposium for Remote Sensing of the Environment (ISRSE), Syndey 2001.

[4] Ferretti, A., Prati, C., and Rocca, F. (2001). "Permanent scatterers in SAR interferometry". *IEEE Transactions on Geoscience and Remote Sensing*, **39(1)**:8–20.

[5] Berardino, P., Fornaro, G., Lanari, R., Sansosti, E. (2002) "A new algorithm for surface deformation monitoring based on small baseline differential SAR interferograms", *IEEE Transactions on Geoscience and Remote Sensing*, **40(11)**: 2375 – 83.

[6] Lazecky, M. (2017) "System for Automatized Sentinel-1 Interferometric Monitoring", 4 pp., P. Soille and P.G. Marchetti (Eds.), Proc. of the 2017 conference on Big Data from Space, ESA, Toulouse, 28-30 Nov 2017, doi:10.2760/383579, JRC108361

[7] ESA (2018) "Sentinel-1 Quality Control: POD – Precise Orbit Ephemerides", available online at https://qc.sentinel1.eo.esa.int

[8] Rosen, P., Gurrola, E., Agram, P. S., Sacco, G. F. and Lavalle, M. (2015). "InSAR Scientific Computing Environment (ISCE): A Python Framework for Earth Science", AGU Fall Meeting 2015.

[9] Geudtner, D., Torres, R., Snoeij, P. and Davidson , M. (2015). "Sentinel-1 System Overview", In ESA Fringe Workshop 2015, Frascati.

[10] ESA (2014) "Sentinel Online: Interferometric Wide Swath", available online at https://sentinel.esa.int/web/sentinel/user-guides/sentinel-1-sar/acquisition-modes/interferometric-wide-swath

[11] Perissin, D. (2015) "SARPROZ software: Official Product Web Page", available online at: http://www.sarproz.com

[12] Hooper A (2008) "A multi-temporal InSAR method incorporating both persistent scatterer and small baseline approaches", *Geophys Res Lett* **35**:L16302. doi:10.1029/2008GL034654, 2008.

[13] O. Tange (2018) "GNU Parallel 2018", DOI:10.5281/zenodo.1146014

[14] Ruiz-Constán, A., Ruiz-Armenteros, A. M., Martos-Rosillo, S., Galindo-Zaldívar, J., Lazecky, M., García, M., Sousa, J. J., et al. (2018) "SAR interferometry monitoring of subsidence in a detritic basin related to water depletion in the underlying confined carbonate aquifer (Torremolinos, southern Spain)", *Science of the Total Environment* **636**: 670-687. DOI: 10.1016/j.scitotenv.2018.04.280.

[15] Goldstein Richard M. and Werner Ch. L. (1998) "Radar interferogram filtering for geophysical applications", *Geophysical Research Letters*, **25**, doi:10.1029/1998GL900033

[16] Lazecký, M. (2018) "Identification of active slope motion in Czech environment using Sentinel-1 interferometry", In: GIS Ostrava 2018, 21-23 Mar 2018, Springer Lecture Notes in Geoinformation and Cartography, 7 p.

[17] Colesanti, C. et al., "SAR Monitoring of Progressive And Seasonal Ground Deformation Using the Permanent Scatterers Technique", Geoscience and Remote Sensing, IEEE Transactions on, vol. 41, no. 7, **2003**, pp. 1685-1701.

[18] Lazecký, M., Bakoň, M., Hlaváčová, I., Sousa, J. J., Real, N., Perissin, D., Patricio, G. (2017) "Bridge Displacements Monitoring using Space-Borne SAR Interferometry", *IEEE Journal of Selected Topics in Applied Earth Observations and Remote Sensing*, **10 (1)**:205-210.

[19] Lazecky, M., Bakon, M., Perissin, D., Papco, J., Gamse, S. (2017) "Analysis of dam displacements by spaceborne SAR interferometry", 9 pp., In: ICOLD 2017, Prague, 3-7 July 2017.

[20] Galve, J.P., Pérez-Peña, J.V., Azañón, J.M., Closson, D., Caló, F., Reyes-Carmona, C., Jabaloy, A., et al. (2017) "Evaluation of the SBAS InSAR Service of the European Space Agency's Geohazard Exploittion Platform (GEP)", *Remote Sensing* **9**, 1291.

[21] Perissin, D. (2017) private communication.

[22] Ruiz-Armenteros, A. M., Lazecky, M., Ruiz-Constán, A., Bakon, M., Delgado, J. M., Sousa, J. J., et al. (2018) "Monitoring continuous subsidence in Costa del Sol (Málaga province, southern Spanish coast) using ERS-1/2, Envisat, and Sentinel-1A/B SAR interferometry", 8 p., Procedia Computer Science, In: CENTERIS, Lisbon, 21-23 Nov 2018.

[23] Ruiz-Armenteros, A. M., Lazecky, M., Hlavacova, I., Bakon, M., Delgado, J. M., Sousa, J. J., et al. (2018) "Deformation monitoring of dam infrastrutures via spaceborne InSAR. The case of La Viñuela (Málaga, southern Spain)", 8 p., In: CENTERIS, Lisbon, 21-23 Nov 2018.